

Article

Influence of Relative Humidity and Oxygen Concentration on Corrosion Behaviour of Copper in H₂S-Containing Liquid Petroleum Gas

Xianqiang Li ¹, Yuan Lu ², Qiang Wei ², Hu Wang ^{1,*} and Juan Xie ^{1,*}¹ School of New Energy and Materials, Southwest Petroleum University, Chengdu 610500, China² CenerTech Oilfield Chemical Co., Ltd., CNOOC, Tianjin 300450, China

* Correspondence: senty78@hotmail.com (H.W.); jennyx99@126.com (J.X.)

Abstract: In this paper, the influences of relative humidity (*RH*) and concentration of O₂ on copper corrosion in H₂S-containing LPG (liquid petroleum gas) were studied. The corrosion products obtained in different environments were also analysed by scanning electron microscopy (SEM), energy dispersive spectrometry (EDS), grazing incidence X-ray diffraction (GIXRD), X-ray photoelectron spectroscopy (XPS) and Fourier transform infrared spectroscopy (FTIR). In H₂S-containing LPG, *RH* has pronounced influence on the corrosion grade of copper. The variation in the critical point (*CP*) with the *RH* of LPG is a linear relationship. The presence of O₂ in dry H₂S has limited influence on the corrosion of copper. In the presence of different *RH*s, the *CP* always follows a negative exponential function with O₂ concentration. The analysis of different corrosion products implies different corrosion behaviours and mechanisms, which are dependent on the presence or absence of water vapour. The corrosion mechanisms obtained in four different environments were also proposed.

Keywords: copper corrosion; liquefied petroleum gas; H₂S corrosion; SEM; XPS



Citation: Li, X.; Lu, Y.; Wei, Q.; Wang, H.; Xie, J. Influence of Relative Humidity and Oxygen Concentration on Corrosion Behaviour of Copper in H₂S-Containing Liquid Petroleum Gas. *Metals* **2022**, *12*, 2015. <https://doi.org/10.3390/met12122015>

Academic Editor: David M. Bastidas

Received: 12 October 2022

Accepted: 17 November 2022

Published: 24 November 2022

Publisher's Note: MDPI stays neutral with regard to jurisdictional claims in published maps and institutional affiliations.



Copyright: © 2022 by the authors. Licensee MDPI, Basel, Switzerland. This article is an open access article distributed under the terms and conditions of the Creative Commons Attribution (CC BY) license (<https://creativecommons.org/licenses/by/4.0/>).

1. Introduction

Natural gas is widely used in industry and our daily life. As an important existence of natural gas, liquefied petroleum gas (LPG) is more commonly utilized for its accessibility in transportation. In the exploitation and processing of LPG, sulphur removal is inevitable for the sake of alleviating corrosion attack by sulphide existing in produced LPG [1–3]. Various forms of sulphide, such as hydrogen sulphide, mercaptan and carbonyl sulphide, may lead to corrosion of copper components in production and storage facilities. Although the sulphur removal process can eradicate most of the sulphide to some extent, the residual sulphide, in trace amounts, can also be harmful to the corrosion of copper components. Of those common active sulphides, H₂S is the most harmful to copper, even it is presented in low concentration. Although previous studies have revealed the behaviour of H₂S on copper corrosion in LPG, the influence of other environmental factors, such as the presence of O₂ and relative humidity (*RH*), also contribute to corrosion attack.

Recently, the corrosion behaviour of copper in the presence of various sulphides has been extensively studied [4–7]. Echeverria investigated the copper corrosion in SO₂ through atomic force microscopy (AFM). The results showed that the microscopic topography and roughness of the copper surface changed after several weeks in a polluted atmosphere containing SO₂ [8]. Majtás discovered that low concentrations of H₂S can corrode copper parts, resulting in electrical failure of electronic equipment. Additionally, the adsorbed water can promote corrosion attack [9]. Zhu proved that the corrosion rate of copper in an SO₂ environment first increases and then gradually decreases with exposure time. Conversely, the corrosion rate of copper in H₂S increases slowly at first and then sharply declines [10]. Araban studied the corrosion behaviour of copper in different rural atmospheres. The results showed that corrosion product of Cu₂O formed preferentially, in which

relative humidity and ammonium sulphate had remarkable influence on the corrosion behaviour [11]. Monzó found that sulphide has an obvious influence on corrosion between the boundary and the centre of a copper sheet. Additionally, elemental sulphur is more corrosive than ethanethiol. The corrosion products of elemental sulphur are in the form of nodule particles, and the ethanethiol is in the form of a uniform film [12]. García found that, at low concentrations of elemental sulphur (5 ppm), mercaptans can significantly promote corrosion. At high concentrations of elemental sulphur (25 ppm), mercaptans inhibit the corrosion of elemental sulphur. Disulphide has an obvious inhibition effect on the corrosion of elemental sulphur [13]. Studies on the corrosion behaviour of copper in the outdoor natural atmosphere have also been reported [14–20]. Kong proved that the uneven corrosion of copper in the atmosphere of Turpan is caused by the dry–wet cycle and the cold–heat cycle [21]. Lopesino believed that the corrosion of copper is more serious when closer to the coast, and the degree of patina coverage depends on the concentration of chloride in the atmosphere [22]. Yan confirmed that the corrosion rate of copper in the atmosphere with sodium chloride is almost 30000 times higher than that in the blank atmosphere [23]. Some other studies focused on the influence of *RH* on the corrosion behaviour of copper [24–26]. Odnevall believed that in the rural atmosphere containing ammonium sulphate, the *RH* of the gas had a great influence on the corrosion behaviour of copper [12]. Sharma proposed that regarding copper in H_2S with low relative humidity, the Cu_2O layer resulted by air has a good protective effect on H_2S . It almost has no protection under high *RH* [27]. Wu proved that the *RH* of the chloride-containing atmosphere is a key factor affecting the corrosion behaviour of copper wires [28]. The corrosion behaviour of chloride on copper has also been extensively studied [29]. Chen proposed that the non-uniform growth of corrosion products on the copper surface in chloride-containing sulphide aqueous solutions resulted in a potential difference between the “thick film” and the “thin film”, and this small potential difference accelerated the occurrence of corrosion [30]. Lu believed that chloride ions in the marine atmosphere of Nansha are the key factors to accelerate the corrosion of copper, and the corrosion products are Cu_2O and $Cu_2Cl(OH)_3$ [31]. Schindelholz believed that sodium chloride is favourable for the formation of NaOH-rich diffusion regions, and copper preferentially forms Cu_2O and $Cu(OH)_2$ [32]. There are also few reports on the electrochemical study of corrosion products on copper surfaces [33]. Tran found that the growth of corrosion product films of copper exposed to H_2S -containing subsurface gas has three successive stages: the first stage is a linear growth rate in thin layers (less than 15 nm). In the second stage, the oxidation rate is limited by the diffusion of copper(I) ions through the thicker corrosion layer. The third stage is linear growth [34]. Fiaud believes that both hydrogen sulphide concentration and relative humidity can promote the growth of oxide and sulphide corrosive substances. The growth mechanism of Cu_2O is an electrochemical mechanism, and the growth mechanism of Cu_2S is a mixed chemical and electrochemical mechanism [35]. Some other reports aimed at the corrosion behaviour of copper regarding other aspects, for example, application of theoretical calculations to copper corrosion [5–7,24], the influence of various organic acids on copper corrosion [36,37], the influence of changes in magnetic field on copper corrosion [38] and corrosion behaviour of copper by oxygen plasma [39].

Although some behaviours of copper corrosion in H_2S have been studied, there is still some insufficiency. It is necessary to investigate the corrosion behaviour and mechanism of copper in LPG containing H_2S at different conditions, including the presence of different *RH*s and O_2 concentrations. In this paper, the influence of *RH* and O_2 on the corrosion behaviour of copper in H_2S -containing LPG was studied, the corrosion products on the surface of copper sheets were characterized and analysed and the corresponding corrosion mechanism of H_2S on copper was proposed.

2. Experimental Methods

2.1. Materials

Copper sheets used in corrosion experiments were purchased from Fushun Keruisi Instrument Co., Ltd. Fushun Liaoning Province, China, which strictly follows the requirement of the ASTM standard [40]. The size of cuboid copper sheet is 75 mm × 12.5 mm × 3 mm, with the purity higher than 99.9%. Copper powder (analytical grade, Chengdu Kelon Chemical Co., Ltd. Chengdu, China) was used in X-ray photoelectron spectroscopy (XPS) and FTIR (Fourier transform infrared spectrometry). The purity of powder is 99.5% and the average particle size is 23 µm. The components of LPG are listed in Table 1. H₂S and O₂ gas used in the experiments were purchased from Zhengrong Gas company (Chengdu, China). The purity of H₂S and O₂ is 99.9%.

Table 1. The components of LPG.

Component	Propane	Isobutane	N-Butane
wt./%	70	14	16

2.2. Copper Corrosion Tests

Copper corrosion tests were carried out according to the ASTM standard [40]. The copper sheet was first abraded with 65 µm silicon carbide sandpaper. Then, it was washed with isooctane. The copper surface was polished by 105 µm silicon carbide particles, which were operated with the assistance of isooctane-soaked degreasing cotton. The prepared copper sheets were suspended into the cylinder (the special closed container for corrosion test) in three parallel experiments. Then, high-purity N₂ was used to remove the air inside the cylinder, by ventilating N₂ into the cylinder to substitute the air. Then, to control the mass flow of LPG and H₂S through a flowmeter (FMA5400A, Omega, San Antonio, TX, USA), they were injected into the cylinder and the gas was mixed evenly. Subsequently, the valve was fastened. Finally, the cylinder with mixture of LPG and H₂S was vertically immersed in a water bath at a constant temperature (40 ± 0.5 °C) for 60 ± 5 min. After the experiment time was over, the liquid and gas in the cylinder were discharged. The copper sheets were taken out and compared with the standard colour plate [40]. Next, the corrosion grades of the copper sheets were evaluated. The details of the grade evaluation are shown in Table 2. The standard stipulates that if the corrosion level of a copper sheet reaches 2a and above, it is regarded as unqualified in corrosion.

Table 2. The grading table of copper corrosion standard swatches [40].

Corrosion Level	Copper Colour	Detailed Description
1	mild discolouration	a. pale orange, almost the same as freshly polished copper b. dark orange a. fuchsia b. lavender
2	moderate discolouration	c. multicoloured with lavender blue, silver or both, overlaid on fuchsia d. silver e. brass or golden yellow
3	deep discolouration	a. multicolour magenta overlay brass b. multicolour (malachite green) shown by red and green, no grey
4	corrosion	a. transparent black, dark grey or brown with only malachite green b. graphite or matte black c. glossy black or jet-black glossy black

2.3. Analysis of Corrosion Products

To facilitate the characterization of corrosion products, the concentrations of H₂S and O₂ were increased to 50 ppm and 10 ppm in copper corrosion tests. The copper sheets were used in corrosion tests for characterizations such as scanning electron microscopy (SEM),

energy dispersive spectrometry (EDS) and grazing incidence X-ray diffraction (GIXRD). Samples of corrosion products for XPS and FTIR were prepared with powder, which could provide better results than copper sheets. The copper powder samples were applied by placing 0.1 g of copper powder in a glass sample bottle. Then, the glass sample bottle was suspended in a cylinder to conduct a copper corrosion experiment.

SEM (Model EVO MA15, ZEISS, Jena, Germany) was used to observe the morphology of the corrosion products on the copper surface. EDS (Model X-MaxN, OXFORD INSTRUMENTS Company, Abingdon, UK) was used to analyse the elemental composition of the corrosion products on the copper sheet surface. XPS (Nexsa type, Thermo Scientific, Waltham, MA, USA) was used to analyse the elemental composition and valence distribution of the corrosion products on the copper powder surface. The original XPS image was fitted with Casa XPS software. GIXRD (SmartLab 9 kw, Rigaku, Tokyo, Japan) was used to analyse the phase composition of corrosion products on the copper sheet surface. FTIR (INVENIO R, Bruker Optik GmbH, Bremen, Germany) was carried out to test the infrared spectrum of the corrosion products on the copper powder surface.

3. Results and Discussion

3.1. Influence of Humidity on Copper Corrosion in H_2S -Containing LPG

The corrosion behaviour of copper in H_2S -containing LPG is very sensitive to the gas humidity. The higher the gas humidity, the more easily copper is corroded by H_2S . Figure 1a shows the variation in the corrosion grade of copper in H_2S -containing LPG at different gas humidities. In LPG containing 3 ppm H_2S , the corrosion grade of copper gradually intensifies with the increase in gas humidity. At 0–30% RH, there is no significant corrosion on the copper surface (corrosion grade is 1a). At 50–100% RH, the surface of the copper sheet begins to corrode (at 50% RH, the copper corrosion grade is 2a). The degree of corrosion varies with humidity. The copper corrosion grade reaches 2e at 100% RH. Meanwhile, the variation in the copper corrosion grade in LPG without H_2S in the presence of different gas humidities is used as comparison, in which the copper surface does not corrode at all humidities (corrosion grade is 1a).

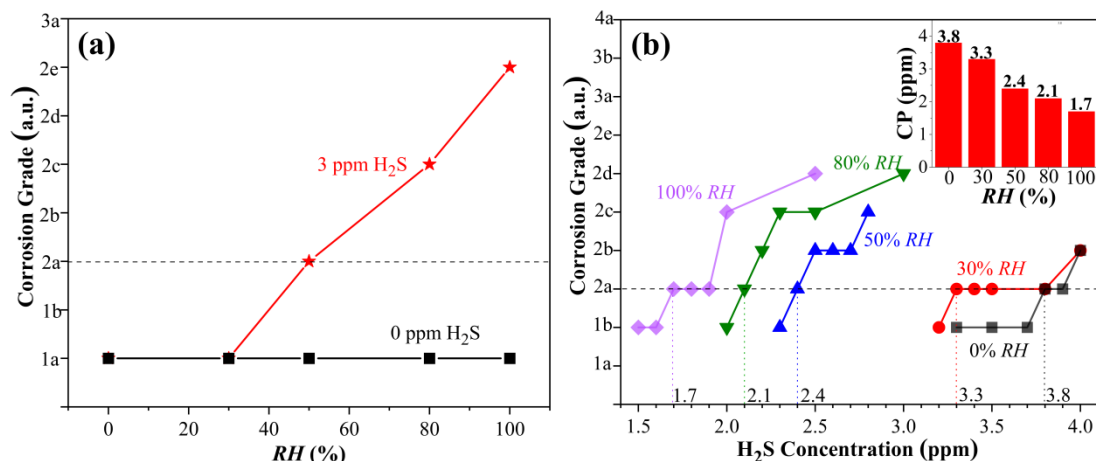


Figure 1. (a) Variation in copper corrosion grade in H_2S -containing LPG with humidity; (b) the influence of H_2S concentration and RH on the corrosion grade of copper in LPG.

The critical point (CP) of copper corrosion in H_2S -containing LPG decreases with the increase in the relative humidity of LPG. The CP is defined as the lowest H_2S concentration to reach the corrosion grade of 2a at specific environmental conditions. Figure 1b shows the influence of H_2S concentration and RH on the corrosion grade of copper in LPG. It can be seen that the CP gradually decreases with the increase in gas humidity. From 0% RH to 100% RH, the CP decreases from 3.8 ppm H_2S to 1.7 ppm H_2S . It indicates that higher humidity is more beneficial to the corrosion process. In higher humidity, the thin film of

water at the copper surface forms more easily, which provides an electrolyte environment for H_2S dissolution and electrochemical corrosion. With the increase in RH , the thickness of the water film at the interface increases, which will provide a better condition for electrochemical corrosion. Therefore, the corrosion attack is more severe at higher RH and the CP would be lowered with the increase in RH .

The influence of RH on the CP is shown in Figure 2. The results of the CP at different RH s show a linear relationship. The fitted data obey Equation (1) as follows:

$$CP = -0.021 RH + 3.77, R_0 = 0.96 \quad (1)$$

where CP is the critical point of copper corrosion, corresponding to the lowest H_2S concentration for reaching the corrosion grade of 2a. RH is the relative humidity for the corrosion test. R is the coefficient of determination. The results imply that with the increase in RH , the thickness of the water film formed at the copper surface increases accordingly. The thicker water film is more favourable for H_2S dissolution. Consequently, the electrochemical corrosion process is enhanced.

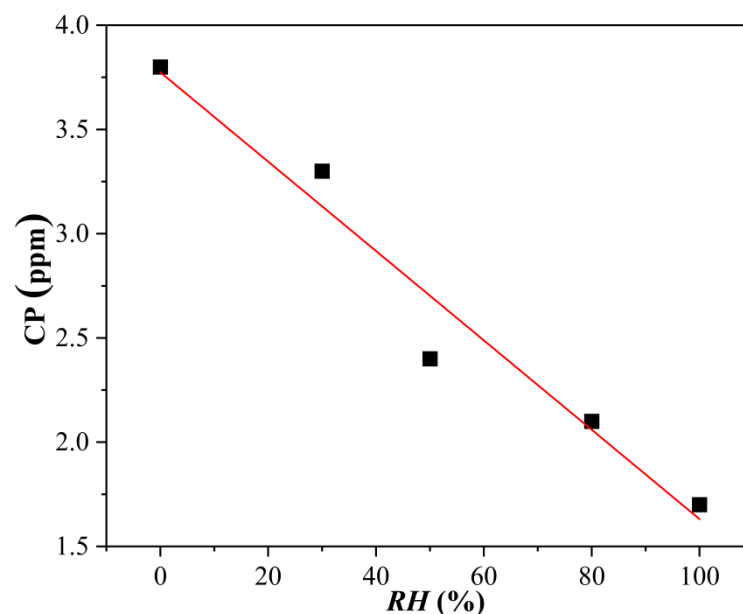


Figure 2. The influence of RH on CP of copper corrosion in H_2S -containing LPG.

3.2. Synergistic Effect of Oxygen and Humidity on Copper Corrosion in H_2S -Containing LPG

A small amount of O_2 has limited influence on the corrosion of copper in dry LPG (0% RH). Figure 3a shows the variation in copper corrosion grade with O_2 content in LPG (0% RH) containing H_2S . As can be seen from Figure 3a, in pure LPG (without H_2S), the corrosion grade of copper does not change with the increase in O_2 content (corrosion grade is 1a). No apparent corrosion happened at the copper surface at such condition. In LPG containing trace H_2S (1 ppm), slight corrosion on the copper surface appears with the increase in O_2 content. Among them, there is no apparent corrosion on the copper surface from 0 to 5 ppm O_2 , and the corrosion grade of copper sheets in 10 ppm O_2 begins to rise to 1b, which is also below 2a.

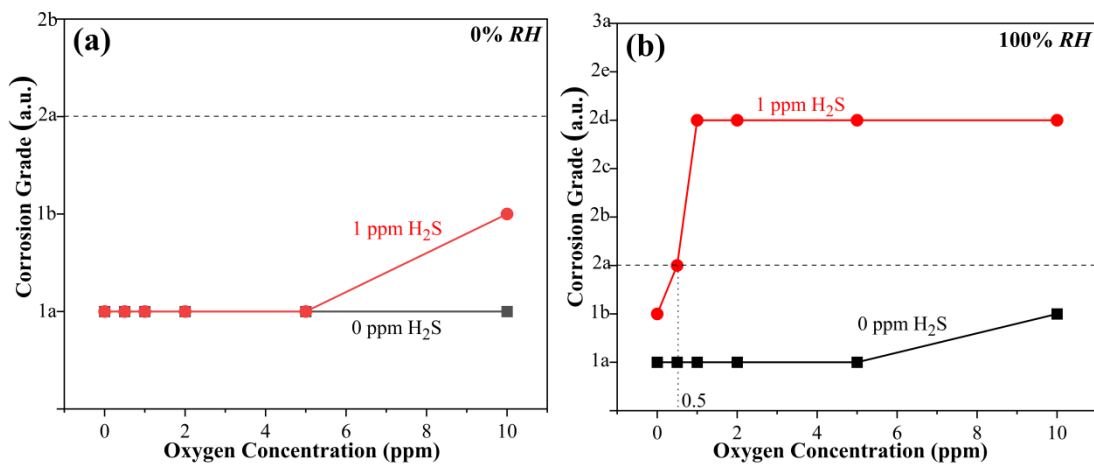


Figure 3. Influence of oxygen concentration on copper corrosion grade in H₂S-containing LPG at (a) 0% RH, (b) 100% RH.

A small amount of O₂ has a pronounced effect on the corrosion of copper in wet LPG (100% RH). Figure 3b is the variation in copper corrosion grade in H₂S-containing LPG (100% RH) with O₂ concentration. It demonstrates that in the absence of H₂S, the copper corrosion grade can hardly be changed with the increase in O₂ content. The copper surface does not corrode in 0–5 ppm O₂, displaying a corrosion grade of 1a. In the presence of 10 ppm O₂, the copper corrosion grade is slightly promoted to 1b. In the presence of a trace amount of H₂S (1 ppm) at 100% RH, the degree of corrosion is sharply intensified with the increase in O₂ content. An amount of 0.5 ppm of O₂ can lead to unqualified copper corrosion (grade 2a). When the O₂ content increases to 1 ppm, the corrosion grade rapidly climbs to grade 2d. When the content of O₂ continues to increase, the corrosion grade is stabilized at grade 2d.

Figure 3 reveals that the coexistence of gas humidity and O₂ has a notable synergistic effect on the corrosion of copper in LPG in the presence of H₂S. Compared with pure LPG (0% RH, 0 ppm O₂), the copper in LPG containing wet H₂S and O₂ is more easily corroded.

In order to further study the synergistic effect of oxygen and humidity on the CP of copper corrosion in H₂S-containing LPG, the corrosion behaviour of copper in H₂S-containing LPG in the presence of different oxygen concentrations was studied at 0% RH, 30% RH, 50% RH, 80% RH and 100% RH, respectively. The results are shown in Figure 4. It can be seen that at every RH condition, the CP gradually decreases with the increase in O₂ concentration. At the same oxygen concentration, CP gradually declines with the increase in the gas humidity.

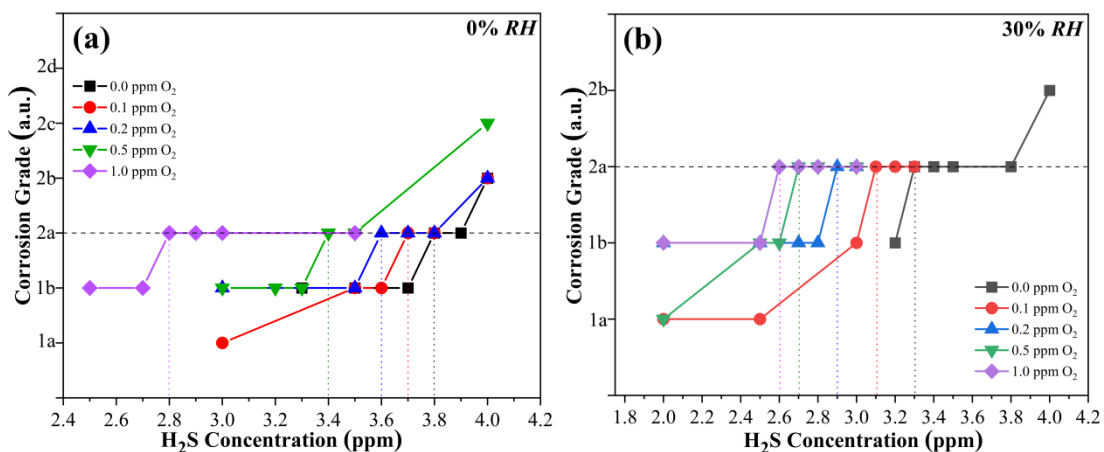


Figure 4. Cont.

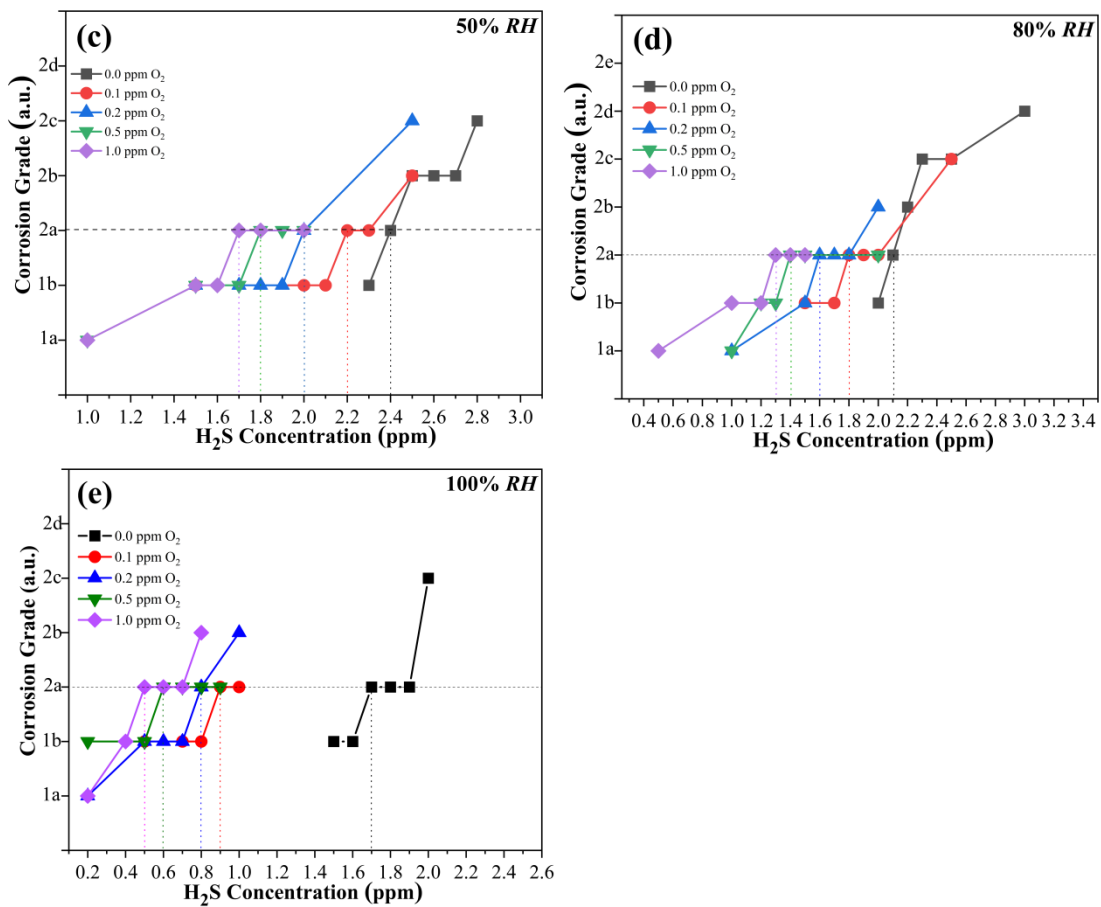


Figure 4. Influence of oxygen content on CP at (a) 0% RH, (b) 30% RH, (c) 50% RH, (d) 80% RH, (e) 100% RH.

More precise behaviour can be illustrated by interpreting the relationship between the CP and O₂ concentration at different RHs, as is shown in Figure 5. The discussion is carried out at different RHs.

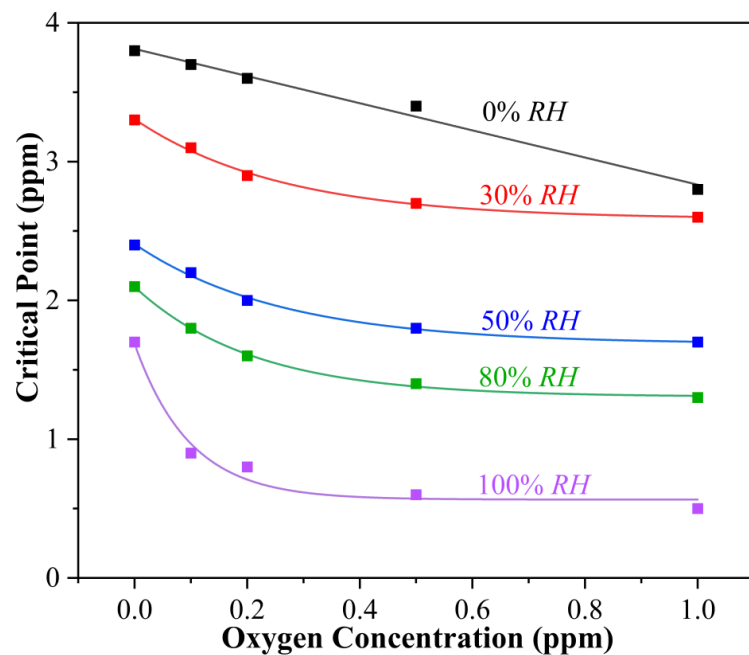


Figure 5. Fitted data of the CP in different LPG environments.

- (a) In the absence of water (0% RH), CP follows a linear relationship with O₂ concentration. The fitted data obey Equation (2) as follows:

$$CP_{0\%} = 3.81 - 0.978 C_0, \quad R_1 = 0.98 \quad (2)$$

where $CP_{x\%}$ is the critical point of copper corrosion in H₂S-containing LPG (x% RH), corresponding to the minimum H₂S concentration for corrosion grade 2a. C_0 is the oxygen concentration of LPG in the copper corrosion test. R is the coefficient of determination.

- (b) In the presence of water (30% RH), CP follows a negative exponential function with the O₂ concentration. The fitted data obey Equation (3) as follows:

$$CP_{30\%} = 0.720 e^{-3.82 C_0} + 2.585, \quad R_2 = 0.99 \quad (3)$$

- (c) In the presence of water (50% RH), CP follows a negative exponential function with the O₂ concentration. The fitted data obey Equation (4) as follows:

$$CP_{50\%} = 0.720 e^{-3.82 C_0} + 1.685, \quad R_3 = 0.99 \quad (4)$$

- (d) In the presence of water (80% RH), CP follows a negative exponential function with the O₂ concentration. The fitted data obey Equation (5) as follows:

$$CP_{80\%} = 0.793 e^{-4.74 C_0} + 1.305, \quad R_4 = 0.99 \quad (5)$$

- (e) In the presence of water (100% RH), CP follows a negative exponential function with the O₂ concentration. The fitted data obey Equation (6) as follows:

$$CP_{100\%} = 1.123 e^{-10.20 C_0} + 0.564, \quad R_5 = 0.98 \quad (6)$$

In the absence of H₂O, the contribution of O₂ to copper corrosion is relatively even, which is consistent with a previous report [27]. However, the presence of H₂O makes copper corrosion more sensitive to O₂ even at low O₂ concentration. The formation of a water film on the copper surface makes the corrosion process different. According to the Arrhenius Equation, Equations (7) and (8), in kinetics, when the temperature of the reaction system is constant, the rate constant of a specific chemical reaction is related to the activation energy of the reaction. The lower the activation energy of the reaction, the faster the reaction rate is. In the presence of H₂O, the activation energy in the reaction system decreases (Equation (9)). Compared with the reaction system without H₂O, the reaction rate constant (k) is larger, so the reaction rate is faster. This explains why the CP at 0% RH is higher than the CP in the presence of H₂O.

$$k_{(0)} = A e^{(-E_{a(0)}/RT)} \quad (7)$$

$$k_{(c)} = A e^{(-E_{a(c)}/RT)} \quad (8)$$

from Equations (7) and (8):

$$E_{a(c)} = E_{a(0)} - RT \ln(k_{(c)}/k_{(0)}) \quad (9)$$

where $k_{(0)}$ is the rate constant of the reaction, $k_{(c)}$ is the rate constant of the reaction after adding the catalyst, $E_{a(0)}$ is the activation energy of the reaction (kJ·mol⁻¹), $E_{a(c)}$ is the activation energy of the reaction after adding the catalyst (kJ·mol⁻¹), A is the pre-exponential factor, e is the natural base (2.718), R is the gas constant (8.314 J·mol⁻¹·K⁻¹) and T is the thermodynamic temperature (K). The presence of the water film, which acts as a catalyst in the system at the interface, changes the kinetics of the corrosion process.

The variation in the CP with O_2 at different RH s can also be explained by Equations (7)–(9). It is well known that the presence of a water film at the interface can reduce the activation of the reaction, which can increase the number of activated molecules in the reaction system by increasing the number of effective collisions. Thus, it significantly accelerates the reaction rate. A higher RH in the reaction system means a thicker water vapour film on the copper surface, which implies greater effectiveness in promoting the corrosion process. When the reaction concentration is constant, the thicker water film can generate more activated molecules in the reaction system, the reaction rate constant (k) is larger and more effective collisions are generated per unit time to form more Cu_2S and Cu_2O .

3.3. Corrosion Mechanism of Copper in Different H_2S -Containing LPG Environments

3.3.1. Surface Morphologies after Corrosion

In different environments, LPG with H_2S , $H_2S + H_2O$, $H_2S + O_2$ and $H_2S + O_2 + H_2O$, the microscopic morphologies of the corrosion products on the copper surface sheet are shown in Figure 6. In the absence of H_2S , the copper surface displays an uncorroded appearance with grooves of abrasion. When corroded in H_2S -containing LPG, the copper surface is evenly covered with a thick corrosion product film. The corrosion products are in the shape of a regular hexagon with sharp edges and corners. In LPG (100% RH) containing $H_2S + H_2O$, the copper surface is evenly covered with a thick layer of corrosion product film. The corrosion products are spherical and accumulate at the grooves of scratches, indicating that the nucleation and growth of corrosion tend to preferentially happen at grooves of scratches [41]. A similar phenomenon also appears in other environments. In $H_2S + O_2$, the amount of corrosion products is significantly reduced. The corrosion products are sporadically distributed on the copper surface. The white particles of corrosion products are irregular in shape and size. It can be seen from the morphology that the general corrosion at this condition is significantly reduced, which is consistent with the previous experimental results. The corrosion attack happens at localized active sites, not on the whole surface. In $H_2S + H_2O$ (100% RH) + O_2 , it exhibits a thick corrosion product film on the copper surface. Some irregular white corrosion products attach on the film surface.

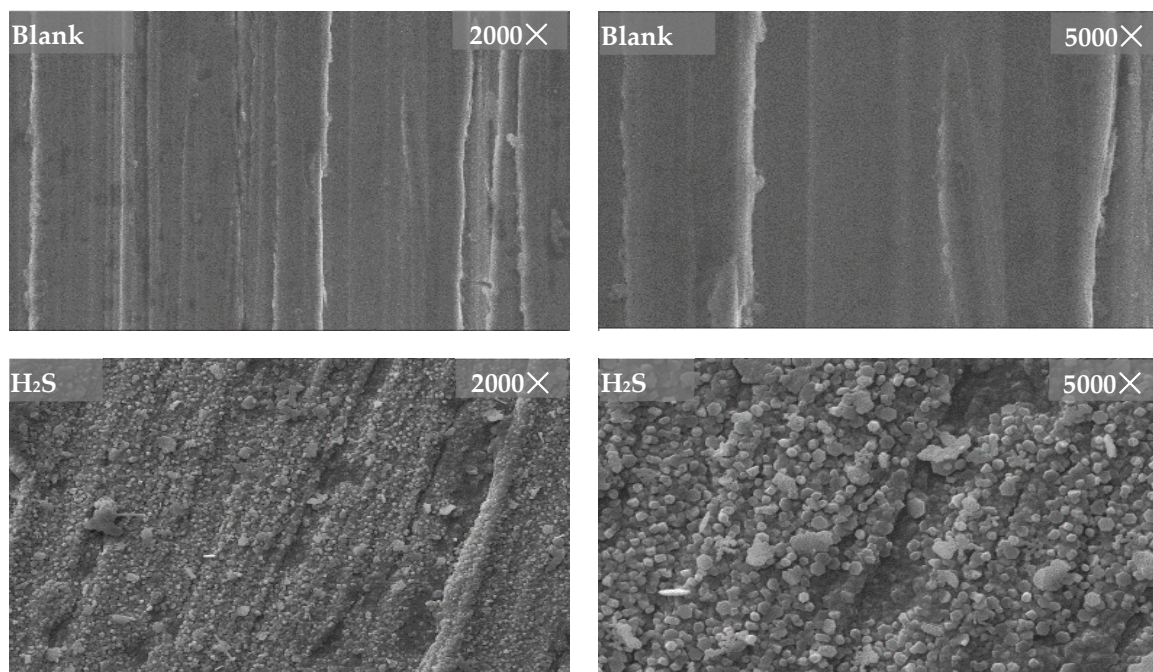


Figure 6. Cont.

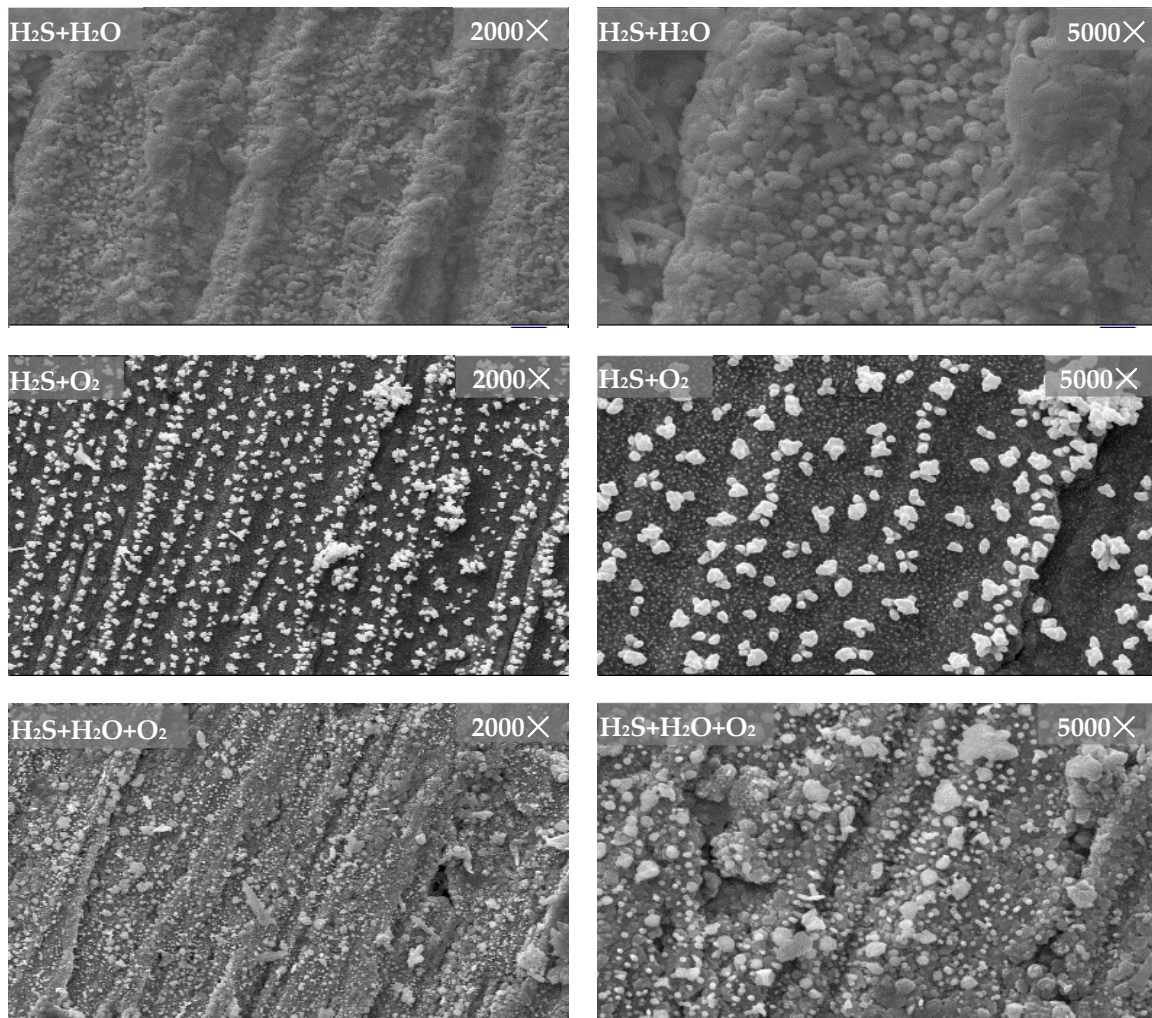


Figure 6. SEM images of corrosion products of copper sheets after corrosion tests in H_2S , $\text{H}_2\text{S} + \text{H}_2\text{O}$, $\text{H}_2\text{S} + \text{O}_2$ and $\text{H}_2\text{S} + \text{O}_2 + \text{H}_2\text{O}$.

3.3.2. EDS Analysis of Corrosion Products

EDS was used to analyse the elemental information of corrosion products. Figure 7 and Table 3 manifest the elemental content of copper corrosion products at four medium conditions (H_2S , $\text{H}_2\text{S} + \text{H}_2\text{O}$, $\text{H}_2\text{S} + \text{O}_2$ and $\text{H}_2\text{S} + \text{H}_2\text{O} + \text{O}_2$). It can be seen from the results that the corrosion products of LPG in H_2S mainly contain S and Cu, indicating that the corrosion products are only composed of copper sulphides. The corrosion products of LPG containing $\text{H}_2\text{S} + \text{H}_2\text{O}$ mainly contain S, Cu and O, implying that they are mainly composed of copper sulphides and oxides. It is also possible that oxides were generated by exposure of the sample to air. The corrosion products in $\text{H}_2\text{S} + \text{O}_2$ mainly contain S, Cu and O. It shows that the content of S is much higher than that of O, indicating that the corrosion products are mainly composed of a large amount of copper sulphides and a small amount of copper oxides. The corrosion products in $\text{H}_2\text{S} + \text{H}_2\text{O} + \text{O}_2$ mainly contain S, Cu and O elements, meaning that the corrosion products are mainly composed of copper oxides and sulphides. The content of O is much higher than that of S, implying that the existence of H_2O and O_2 is more favourable for the growth of copper oxide. In the presence of H_2O (100% RH), it is more favourable to form a water film on the copper surface, which in turn leads to the dissolution and diffusion of oxygen. The electrochemical corrosion happens with the cathode process of oxygen depolarization reaction. Additionally, the dissolution of H_2S in water film leads to the emergence of H^+ . The hydrogen depolarization reaction

as a cathodic process also happens. The two cathodic processes occur at the same time in $\text{H}_2\text{S} + \text{O}_2 + \text{H}_2\text{O}$, which induces the synergistic corrosion effects.

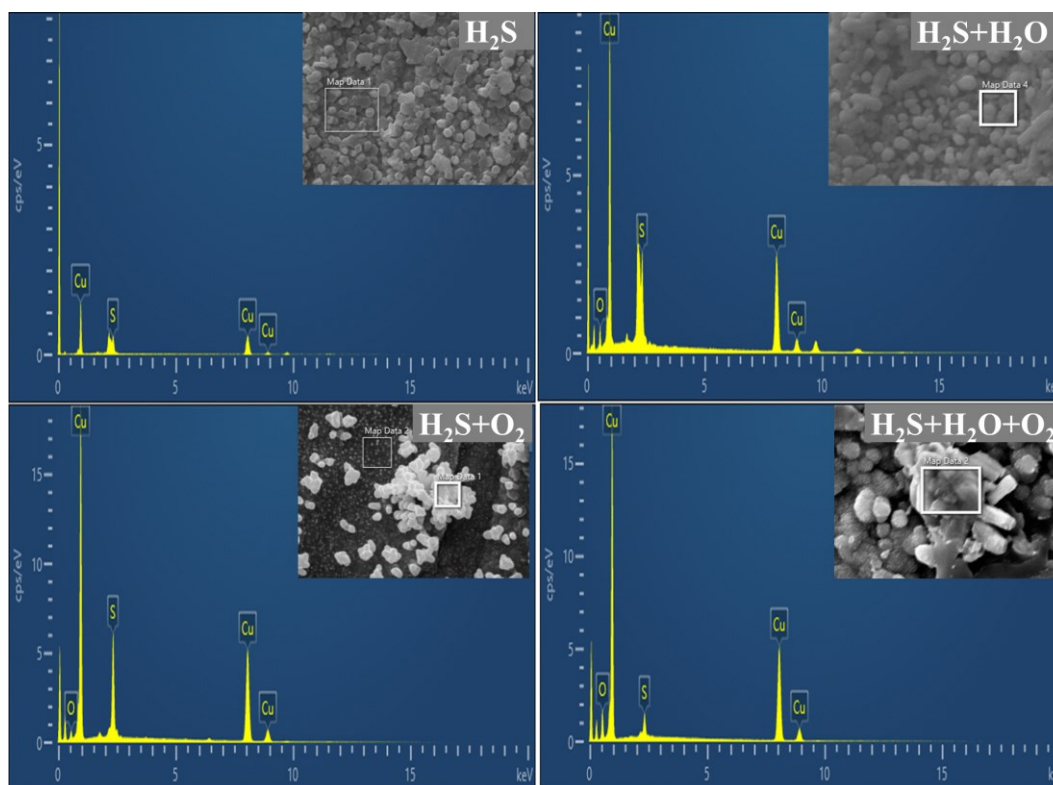


Figure 7. EDS images of corrosion products in different LPG environments.

Table 3. The elemental content of corrosion products at four different corrosion conditions.

Element	H_2S		$\text{H}_2\text{S} + \text{H}_2\text{O}$		$\text{H}_2\text{S} + \text{O}_2$		$\text{H}_2\text{S} + \text{O}_2 + \text{H}_2\text{O}$	
	wt.%	Atomic%	wt.%	Atomic%	wt.%	Atomic%	wt.%	Atomic%
O	-	-	5.18	16.61	2.85	9.20	8.40	25.99
S	9.94	17.95	8.66	13.85	14.98	24.10	3.50	5.40
Cu	90.06	82.05	86.15	69.53	82.17	66.70	88.09	68.60
Total	100.00	100.00	100.00	100.00	100.00	100.00	100.00	100.00

3.3.3. GIXRD Analysis of Corrosion Products

In order to further reveal the corrosion mechanism of copper sheets in different LPG environments, GIXRD was used to analyse the corroded copper sheets in the presence of H_2S , $\text{H}_2\text{S} + \text{H}_2\text{O}$, $\text{H}_2\text{S} + \text{O}_2$ and $\text{H}_2\text{S} + \text{H}_2\text{O} + \text{O}_2$, respectively, and the incident angle of GIXRD was 0.7° . The results in Figure 8 show that the spectrum of corroded copper in H_2S -containing LPG is mainly the diffraction peaks of Cu and Cu_2S , in which Cu_2S preferentially grows on the (-536) crystal plane. The spectrum of corroded copper in LPG containing $\text{H}_2\text{S} + \text{H}_2\text{O}$ is mainly the diffraction peaks of Cu and Cu_2S , in which Cu_2S preferentially grows on the (-232) crystal plane. The expected spectrum of Cu_2O cannot be obtained, which has been proven by EDS. This is due to a too little amount of corrosion products. The spectrum of corrosion products in LPG containing $\text{H}_2\text{S} + \text{O}_2$ is similar to the diffraction peaks of corrosion products at H_2S conditions, mainly Cu and Cu_2S diffraction peaks. Similarly, Cu_2S grows preferentially on the (-536) crystal plane. The spectrum of corrosion products in LPG containing $\text{H}_2\text{S} + \text{O}_2 + \text{H}_2\text{O}$ is mainly Cu, Cu_2S and Cu_2O . The diffraction peak of Cu_2O is obviously stronger than that of Cu_2S , indicating that

the conditions are more preferable to the growth of Cu_2O [34,35,42]. In addition, in this circumstance Cu_2S preferentially grows along the (034) crystal plane, which is different from other environmental conditions.

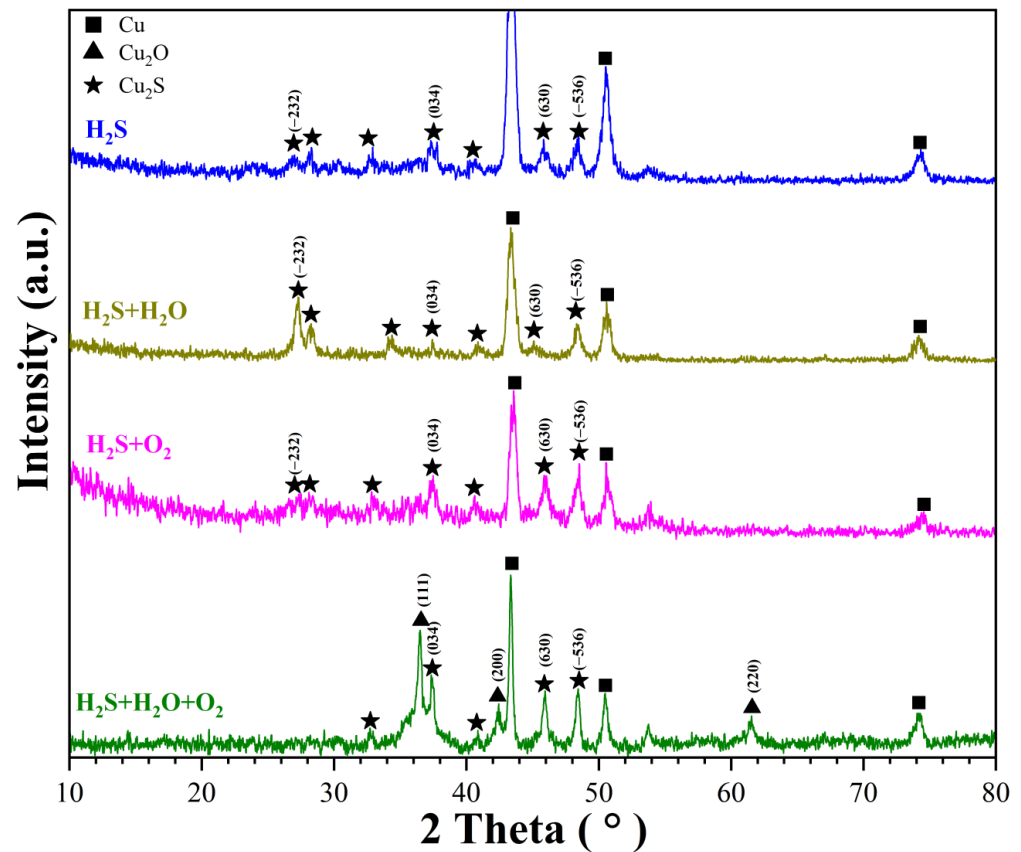


Figure 8. GIXRD patterns of corrosion products at different conditions.

3.3.4. XPS Analysis of Corrosion Products

XPS was also applied to analyse the valence states of corrosion products of copper sheets in different LPG environments, including H_2S , $\text{H}_2\text{S} + \text{H}_2\text{O}$, $\text{H}_2\text{S} + \text{O}_2$ and $\text{H}_2\text{S} + \text{H}_2\text{O} + \text{O}_2$. The results are shown in Figure 9. Figure 9a is a comparison diagram of the Cu 2p spectrum of the corrosion products in different LPG environments. In the Cu 2p spectrum of the corrosion products in H_2S , the peaks at 932.75 eV and 945 eV correspond to the characteristic peak of Cu_2S and the satellite peak of Cu^+ at the 2p_{3/2} orbital, respectively. The peaks at 932.77 eV, 934.10 eV and 943.00 eV in Cu 2p spectrum of corrosion products in $\text{H}_2\text{S} + \text{H}_2\text{O}$ correspond to the characteristic peaks of Cu_2S , CuO and the satellite peaks of Cu^{2+} at the 2p_{3/2} orbital, respectively. The peaks at 932.70 eV, 934.27 eV and 943.00 eV in the Cu 2p spectrum of corrosion products in $\text{H}_2\text{S} + \text{O}_2$ correspond to the characteristic peaks of Cu_2S , CuO and the satellite of Cu^{2+} at the 2p_{3/2} orbit, respectively. The peaks at 932.80 eV, 932.51 eV and 945.00 eV in the Cu 2p spectrum of the corrosion products with $\text{H}_2\text{S} + \text{H}_2\text{O} + \text{O}_2$ correspond to the characteristic peaks of Cu_2S , Cu_2O and the satellite of Cu^+ at the 2p_{3/2} orbital, respectively, which are consistent with the XRD results. Figure 9b is the analysis result of the high-resolution S 2p spectrum. As seen in Figure 9b, in different LPG environments, the XPS signal of S is weak and exists in the form of Cu_2S .

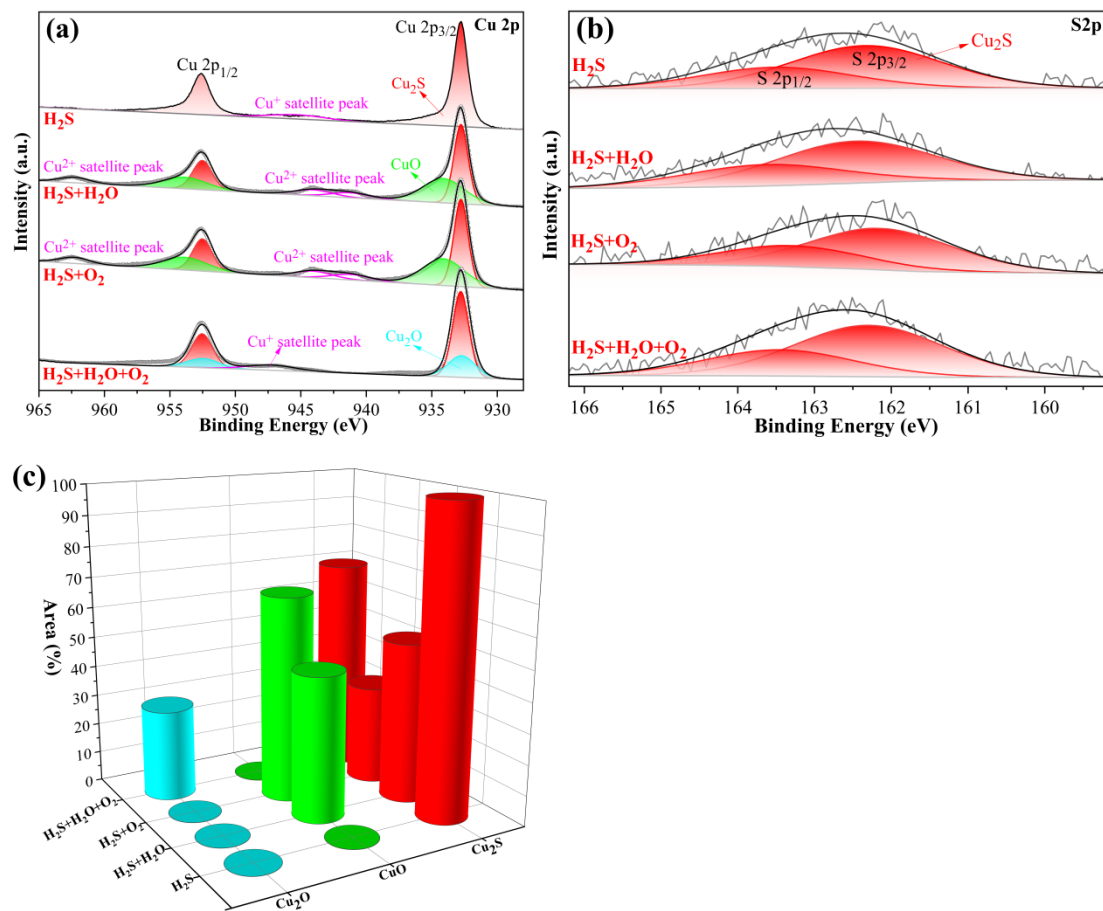


Figure 9. XPS images of corrosion products in different LPG environments: (a) Cu 2p data and fits; (b) S 2p data and fits; (c) the content ratio of each phase in Cu 2p spectrum.

Figure 9c shows the comparative analysis results of the content of Cu₂S, Cu₂O and CuO in the Cu 2p spectrum in different LPG environments. The detailed information of each phase is shown in Table 4. It can be seen from Figure 9c that Cu₂S exists in all four conditions, and the proportion is the highest in pure H₂S. With the addition of H₂O and O₂, the content of Cu₂S decreases and the content of CuO increases gradually. In the presence of H₂O + O₂, Cu₂S content begins to rise again, and Cu₂O appears in large quantities, which agrees with the previous EDS and XRD results.

Table 4. The content ratio of each phase in the corrosion products in the Cu 2p spectrum.

Element	Peak Type	Condition	BE (ev)	Area%
Cu	Cu ₂ S	H ₂ S	932.75	100.00
		H ₂ S + H ₂ O	932.77	52.74
		H ₂ S + O ₂	932.70	32.56
		H ₂ S + H ₂ O + O ₂	932.80	70.26
Cu	Cu ₂ O	H ₂ S	-	-
		H ₂ S + H ₂ O	-	-
		H ₂ S + O ₂	-	-
		H ₂ S + H ₂ O + O ₂	932.51	29.74
Cu	CuO	H ₂ S	-	-
		H ₂ S + H ₂ O	934.10	47.26
		H ₂ S + O ₂	934.27	67.44
		H ₂ S + H ₂ O + O ₂	-	-

3.3.5. FTIR Analysis of Corrosion Products

FTIR was used to analyse the corrosion products in different LPG environments. The results are shown in Figure 10. It compares the FTIR spectra of copper powder and copper powder with four different corrosion products. The full FTIR spectra of all corrosion products are similar to the blank. The absorption peak at 3743 cm^{-1} represents the stretching vibration absorption peak of free-state O-H in the impurities on the copper powder surface. Compared with the blank, the weakening of the peak intensity is caused by the accumulation of a thick layer of corrosion products on the copper powder surface. Compared with blank, the absorption peak of 3446 cm^{-1} is a composite peak, which is composed of a stretching vibration absorption peak of the associative O-H and Cu(I)-S on the copper powder surface. The phenomenon of increased peak intensity is due to the presence of a large amount of Cu_2S (3470 cm^{-1}) after corrosion. The absorption peaks of 2923 cm^{-1} and 2854 cm^{-1} represent the stretching vibration absorption peaks of the C-H bond in the methylene group. The phenomenon of peak intensity enhancement is caused by the residual LPG in the corrosion products. In the FTIR spectrum of the blank, there are many unknown absorption peaks around 1500 cm^{-1} , which should be caused by impurities of the copper powder surface. Figure 10b is an FTIR comparison of $920\text{--}1230\text{ cm}^{-1}$. Compared with the blank, the absorption peak at 1160 cm^{-1} is significantly enhanced, which can be attributed to the stretching vibration of Cu(I)-S (1145 cm^{-1}). The reason why the peak intensity at this position is similar to the blank can be ascribed to little corrosion products on the copper powder surface in $\text{H}_2\text{S} + \text{O}_2$. Compared with the blank, the peak position of 1081 cm^{-1} appears blue-shifted, which is caused by the vibration of a large amount of Cu(I)-S (1115 cm^{-1}). This phenomenon is more pronounced in conditions with more corrosion products. Figure 10c shows the FTIR comparison between 400 cm^{-1} and 800 cm^{-1} for the four corrosion products and the blank. Compared with the blank, the apparent enhancement of the absorption peak at 713 cm^{-1} is due to the in-plane rocking vibration of C-H in the methylene group of the residual LPG adsorbed in the corrosion product. As for the weak absorption peak at 619 cm^{-1} in H_2S and $\text{H}_2\text{S} + \text{H}_2\text{O}$, it can be regarded as the stretching vibration peak of Cu(I)-S (618 cm^{-1}). In $\text{H}_2\text{S} + \text{O}_2$ and $\text{H}_2\text{S} + \text{H}_2\text{O} + \text{O}_2$, a strong absorption characteristic peak at 619 cm^{-1} can be regarded as the composite absorption peak of Cu_2S and Cu_2O (the absorption peak positions of Cu(I)-S (618 cm^{-1}) and Cu(I)-O (614 cm^{-1}) are very similar). The strong absorption peak at 499 cm^{-1} is due to the stretching vibration of $\text{Cu}=\text{O}$ [42–45].

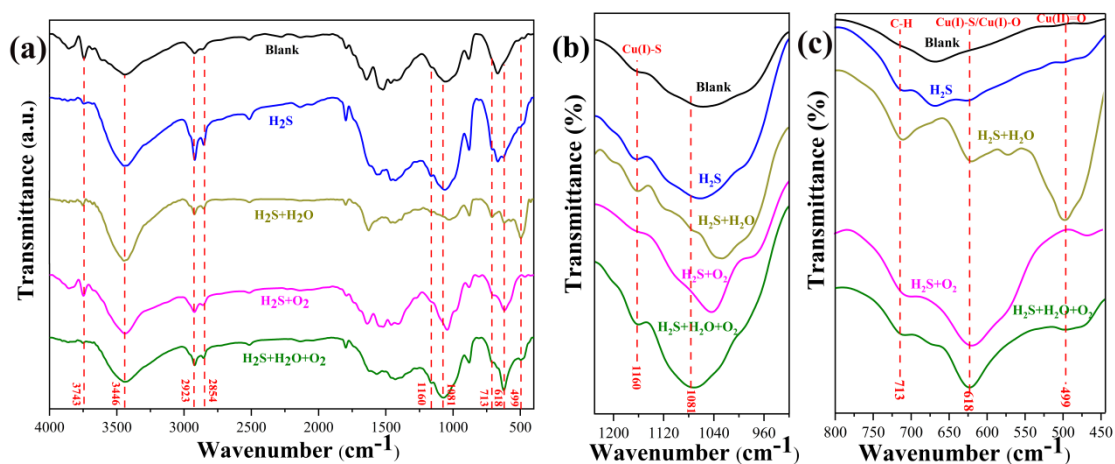


Figure 10. FTIR images of corrosion products on copper powder in different LPG environments: (a) FTIR full spectrum, (b) FTIR images of $920\text{--}1230\text{ cm}^{-1}$, (c) FTIR images of $445\text{--}800\text{ cm}^{-1}$.

The results of the analysis on the differences in the absorption peaks in the FTIR reveal that Cu_2S will be formed on the copper surface in the four conditions. The presence of H_2O promotes the production of CuO .

3.4. Corrosion Mechanism of Copper in Different LPG Environments

Based on the results of copper corrosion tests and corrosion product analysis, the copper corrosion mechanisms of copper at different LPG environments can be proposed as follows.

3.4.1. Corrosion Mechanism in H₂S

The corrosion mechanism of copper in LPG only containing H₂S is a chemical corrosion process. The corrosion process is carried out according to the reaction Equations (10) and (11). Figure 11 is a schematic diagram of the corrosion steps in H₂S-containing LPG. In the first step, H₂S gas in the LPG is adsorbed on the copper surface. Then, H₂S reacts with Cu atoms at the surface to generate H₂ and Cu₂S. The whole corrosion process is a chemical process. Electrochemical corrosion cannot occur due to the absence of the electrolyte.

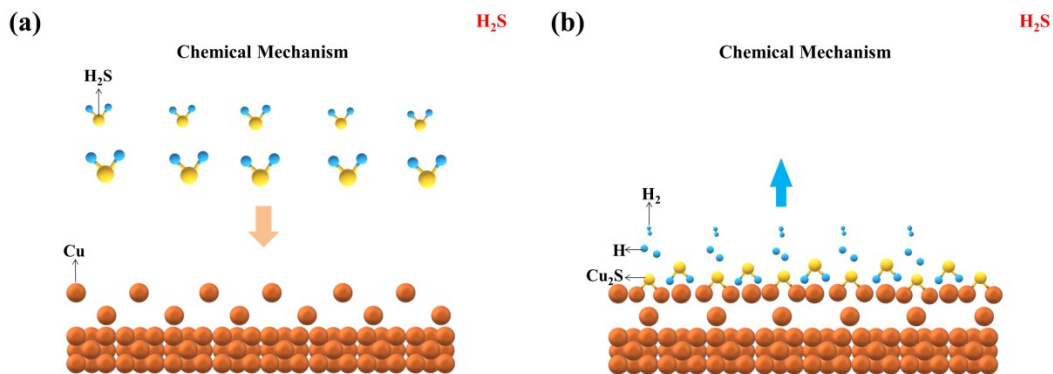
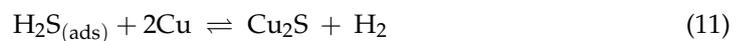


Figure 11. Schematic diagram of corrosion steps of copper sheet in H₂S-containing LPG. (a) step1. (b) step2.

3.4.2. Corrosion Mechanism in H₂S+H₂O

The corrosion mechanism of copper in LPG containing H₂S + H₂O is an electrochemical corrosion process. The corrosion process is carried out according to the reaction Equations (12)–(16). Figure 12 shows the schematic corrosion steps in LPG with H₂S + H₂O. The process of electrochemical corrosion can be explained by Figure 12a–c. Firstly, H₂O exists in the form of a water film on the copper surface. H₂S in LPG dissolves into the water film and further hydrolyses to form a great amount of HS[−], H₃O⁺ (hydronium ions) and a small amount of S^{2−}. Furthermore, the process of the anodic reaction is losing electrons of a Cu atom to form Cu₂S with S^{2−}, as expressed in Equation (15). The cathodic reaction can be undertaken as Equation (16), which is the traditional hydrogen depolarization reaction. At this time, the massive consumption of S^{2−} further promotes the dissolution and hydrolysis of H₂S in LPG, which continuously accelerates the corrosion of copper and results in a great amount of Cu₂S precipitation. However, when the water film is insufficient (low humidity), it is difficult to form an effective electrochemical corrosion environment. In this circumstance, the chemical process may be the main reason for corrosion. This is consistent with the results of XRD, XPS and FTIR. A small amount of CuO in XPS and FTIR is likely due to the contamination of oxidation in air.



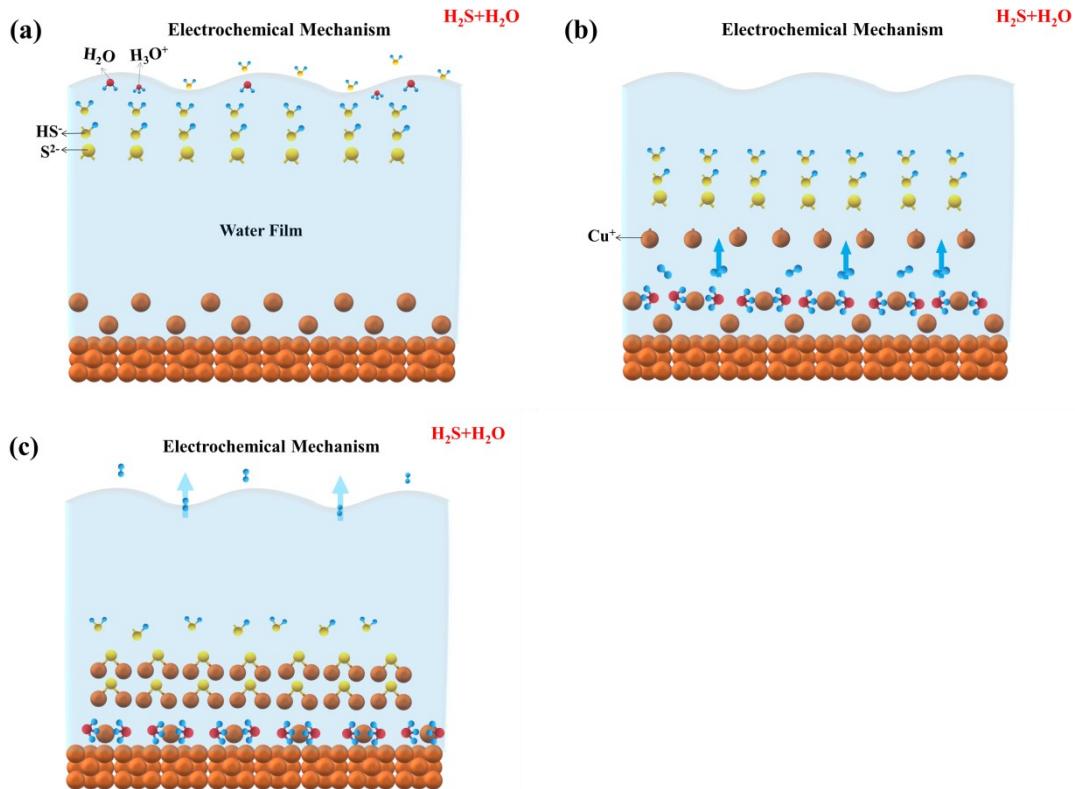
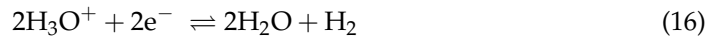


Figure 12. Schematic diagram of corrosion steps of copper sheet in LPG with H₂S+H₂O. (a) step1. (b) step2. (c) step3.

3.4.3. Corrosion Mechanism in H₂S + O₂

The corrosion mechanism of copper in LPG with H₂S + O₂ is a chemical corrosion process. The corrosion process is carried out according to Equations (10), (11) and (17)–(19). Figure 13 displays a schematic diagram of the corrosion process in LPG containing H₂S + O₂. In the first step, H₂S and O₂ molecules in LPG adsorb on the copper surface. Then, the chemical reaction of copper with H₂S and O₂ molecules generate Cu₂S, H₂ and Cu₂O, respectively. Part of Cu₂O is further oxidized to CuO by O₂. The corrosion mechanism shows that the presence of only O₂ will not significantly promote the corrosion grade of the copper sheet, which is consistent with the experimental results. In this condition, the peak of CuO does not appear in the XRD results. However, a small amount of CuO was detected in XPS, indicating that the content of CuO is quite low in corrosion products. With the FTIR spectrum, the amount of Cu₂O is significantly more than CuO, which implies Cu₂O is more stable than CuO.



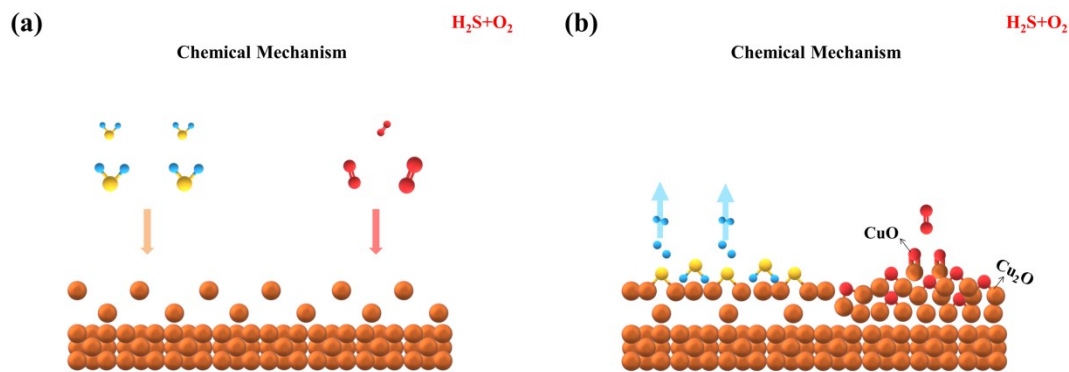
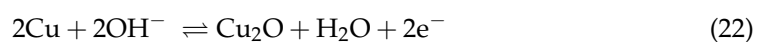


Figure 13. Schematic diagram of corrosion steps of copper sheet in LPG with $\text{H}_2\text{S} + \text{O}_2$. (a) step1. (b) step2.

3.4.4. Corrosion Mechanism in $\text{H}_2\text{S} + \text{H}_2\text{O} + \text{O}_2$

The corrosion mechanism of copper in LPG containing $\text{H}_2\text{S} + \text{H}_2\text{O} + \text{O}_2$ is an electrochemical corrosion process. The corrosion process is carried out according to the Equations (12)–(16) and (20)–(22). The electrochemical corrosion process can be illustrated by the schematic diagram in Figure 14. Firstly, H_2O in LPG exists in the form of a water film on the copper surface. Two electrochemical reactions happen at the interface. The dissolution of H_2S in the water film leads to the electrochemical reaction in Equations (12)–(16). Meanwhile, the dissolution and diffusion of O_2 also cause another electrochemical corrosion reaction, as in Equations (20)–(22), which is the oxygen depolarization process. After H_2S and O_2 molecules in LPG dissolve into the water film to form $\text{H}_2\text{S}_{(l)}$ and $\text{O}_{2(l)}$, $\text{H}_2\text{S}_{(l)}$ is further hydrolysed into a large amount of HS^- , H_3O^+ and a small amount of S^{2-} . Cu loses electrons to form Cu_2S and Cu_2O with S^{2-} and OH^- , according to the anodic reaction of Equations (15) and (22) [46]. H_3O^+ and $\text{O}_{2(l)}$ obtain electrons from copper to form H_2 , H_2O and OH^- , which are regarded as cathode reactions (Equations (16) and (21)) [34,35,47]. Because the H_3O^+ in the water is consumed in large quantities, it is conducive to the ionization of water to move to the right to generate a large amount of OH^- , which increases the pH of the water film. A large amount of OH^- is not only conducive to the dissolution of H_2S in LPG in the water film, improving the solubility of H_2S , but is also conducive to the continuous hydrolysis of $\text{H}_2\text{S}_{(l)}$ and HS^- in the water film to form a large amount of HS^- and S^{2-} , which promotes the formation of lots of Cu_2S precipitates. Thereby, the solubility of H_2S in the water film is further increased to promote the corrosion of copper by H_2S . Figure 14a–c are schematic diagrams of corrosion steps in LPG containing $\text{H}_2\text{S} + \text{H}_2\text{O} + \text{O}_2$. Combined with the previous theoretical analysis and Figure 14, it is shown that when both O_2 and H_2O exist in LPG, the corrosion grade of copper will be significantly increased. A large amount of Cu_2S and Cu_2O will be generated, which is consistent with the previous experimental results of the synergistic effect of humidity and O_2 . Moreover, Cu_2O is thermodynamically more stable than Cu_2S (the standard free energies of formation at room temperature for Cu_2O and Cu_2S are -34.98 and -20.6 kcal/mole, respectively [27]), indicating that Cu_2O is preferentially formed at the same conditions. Therefore, the amounts of corrosion products in Cu_2O are more than Cu_2S . This conclusion is consistent with the results of XRD and EDS. In addition, a large amount of Cu_2O in XPS and FTIR also proves it.



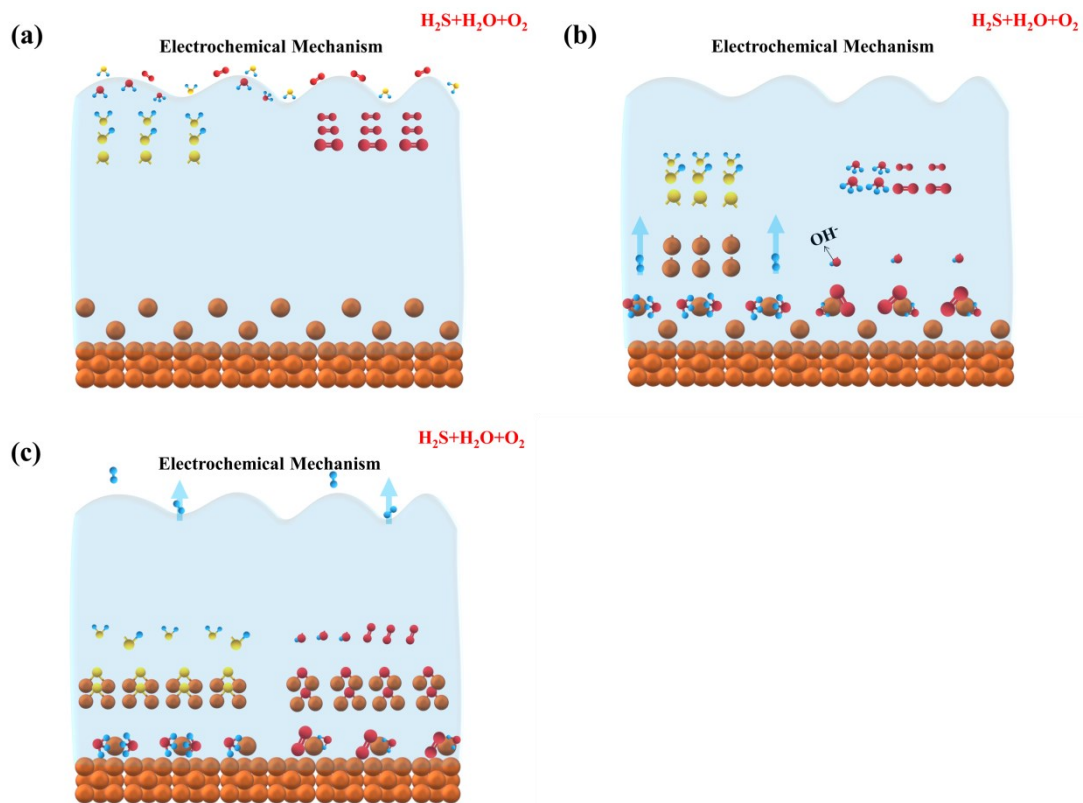


Figure 14. Schematic diagram of corrosion steps of copper sheet in LPG with $H_2S + H_2O + O_2$. (a) step1. (b) step2. (c) step3.

4. Conclusions

In this paper, the influence of humidity and O_2 on copper corrosion in H_2S -containing LPG was studied. The corrosion products were characterized and analysed to reveal the corrosion mechanism. The following conclusions were obtained:

1. In H_2S -containing LPG, RH has pronounced influence on the corrosion grade of copper. The variation in the CP with RH in LPG is a linear relationship.
2. The presence of O_2 in dry H_2S has limited influence on the corrosion of copper. The CP decreases linearly with the increase in O_2 concentration. In the presence of different RH s, the CP always follows a negative exponential function with O_2 concentration.
3. Surface morphologies of corrosion products obtained in different environments are quite different. Gas humidity and the presence of O_2 notably affect the microscopic morphology of corrosion products. In individual H_2S , the morphology of copper corrosion products is a regular hexagon block with sharp edges and corners. In $H_2S + H_2O$ (100% RH), the morphology of copper corrosion products is uniform spherical shape. In $H_2S + O_2$, the morphology of copper corrosion products is irregular in shape and size. In $H_2S + H_2O + O_2$, the morphology of the corrosion products is a regular hexagon block with sharp edges and corners, spherical and irregular in shape and size.
4. In H_2S -containing LPG, RH and O_2 have obvious influence on the composition and distribution of corrosion products. In individual H_2S , the corrosion product of copper is only Cu_2S . In $H_2S + H_2O$, corrosion products of copper are mainly Cu_2S . In $H_2S + O_2$, corrosion products of copper are composed of a large amount of Cu_2S and a small amount of CuO and Cu_2O . In $H_2S + H_2O + O_2$, corrosion products are composed of a large amount of Cu_2O , Cu_2S and a small amount of CuO .
5. The corrosion mechanism of copper in LPG in the presence of different corrosive gases was proposed. The corrosive gas influences the corrosion mechanism remarkably. In individual H_2S and $H_2S + O_2$, the corrosion process is chemical in nature. H_2S and O_2

react with copper directly at the interface. The corrosion mechanism of copper in LPG containing $\text{H}_2\text{S} + \text{H}_2\text{O}$ and $\text{H}_2\text{S} + \text{H}_2\text{O} + \text{O}_2$ is an electrochemical corrosion process. In $\text{H}_2\text{S} + \text{H}_2\text{O}$, the corrosion proceeds with an anodic reaction of copper oxidization and a cathodic reaction of traditional hydrogen depolarization. In $\text{H}_2\text{S} + \text{H}_2\text{O} + \text{O}_2$, two different electrochemical reactions happen: one is the same as in $\text{H}_2\text{S} + \text{H}_2\text{O}$, and the other electrochemical reaction displays as the corrosion of O_2 in neutral medium, in which the cathodic process is oxygen depolarization.

Author Contributions: Conceptualization, H.W. and J.X.; methodology, H.W.; validation, H.W., X.L. and J.X.; formal analysis, Q.W.; investigation, Y.L.; writing—original draft preparation, X.L.; writing—review and editing, X.L.; supervision, H.W. All authors have read and agreed to the published version of the manuscript.

Funding: This research received no external funding.

Institutional Review Board Statement: Not applicable.

Informed Consent Statement: Not applicable.

Data Availability Statement: Not applicable.

Conflicts of Interest: The authors declare no conflict of interest.

References

1. Wang, B.W.; Jiang, Z.M.; Hu, X.C.; Guo, B.L. Discussion on corrosion control of LPG copper sheet in a terminal plant of Bohai oil field. *Chem. Manag.* **2015**, *21*, 3.
2. Yi, F.; Lu, Y.; Zhao, J.M. Influence and mechanism of sulfide in liquefied petroleum gas on copper corrosion. *J. Beijing Univ. Chem. Technol. (Nat. Sci. Ed.)* **2021**, *48*, 59–65.
3. Zhong, X.Y. *Research on Sulfur Corrosion and Removal of Light Oil Products*; China University of Petroleum: Beijing, China, 2011.
4. Halldin Stenlid, J.; Campos dos Santos, E.; Johansson, A.J.; Pettersson, L.G.M. Properties of interfaces between copper and copper sulphide/oxide films. *Corros. Sci.* **2021**, *183*, 109313. [[CrossRef](#)]
5. Long, Y.; Song, W.; Fu, A.; Xie, J.; Feng, Y.; Bai, Z.; Yin, C.; Ma, Q.; Ji, N.; Kuang, X. Combined effect of hydrogen embrittlement and corrosion on the cracking behaviour of C110 low alloy steel in O_2 -contaminated H_2S environment. *Corros. Sci.* **2022**, *194*, 109926. [[CrossRef](#)]
6. Johnsen, R.; Lange, T.; Stenerud, G.; Olsen, J.S. Environmentally assisted degradation of spinodal copper alloy C72900. *Corros. Sci.* **2018**, *142*, 45–55. [[CrossRef](#)]
7. Dou, W.; Jia, R.; Jin, P.; Liu, J.; Chen, S.; Gu, T. Investigation of the mechanism and characteristics of copper corrosion by sulphate reducing bacteria. *Corros. Sci.* **2018**, *144*, 237–248. [[CrossRef](#)]
8. Echeverria, F.; Botero, C.A.; Correa, E.; Meza, D.; Castano, J.G.; Gomez, M.A. High resolution morphological changes of Cu, Ni, Al, and Au surfaces due to atmospheric corrosion. *IEEE Trans. Device Mater. Reliab.* **2017**, *17*, 331–339. [[CrossRef](#)]
9. Majtás, D.; Kreislová, K.; Turek, L. Failure of electric products by H_2S . *Koroze Ochr. Mater.* **2018**, *62*, 71–77. [[CrossRef](#)]
10. Zhu, Z.; Zuo, X.; Ying, Z. Corrosion analysis of copper T2 exposed to polluted atmospheres and study on prediction model. *Corros. Rev.* **2017**, *35*, 35–46. [[CrossRef](#)]
11. Odnevall, I. Atmospheric corrosion of copper in a rural atmosphere. *J. Electrochem. Soc.* **1995**, *142*, 3682–3689. [[CrossRef](#)]
12. Monzó, J.; García-Antón, J.; Guiñón, J.L. Influence of elemental sulphur and mercaptans on corrosion of copper strips in the ASTM D-130 test by means of electronic microscopy (SEM) and energy dispersive X-ray (EDX). *Fresenius J. Anal. Chem.* **1991**, *341*, 606–610. [[CrossRef](#)]
13. Monzó, J.; García-Antón, J.; Guiñón, J.L. Study of corrosion on copper strips by mixtures of mercaptans, sulphides and disulphides with elemental sulphur in the ASTM D-130 test by means of electron microscopy (SEM) and energy dispersive X-ray (EDX). *Fresenius J. Anal. Chem.* **1992**, *343*, 593–596. [[CrossRef](#)]
14. Toyoda, E.; Watanabe, M.; Higashi, Y.; Tanaka, T.; Miyata, Y.; Ichino, T. Depth profiling analysis of tarnish films on copper formed during short-term outdoor exposure by glow discharge optical emission spectroscopy. *Corrosion* **2004**, *60*, 729–735. [[CrossRef](#)]
15. Graedel, T.E.; Franey, J.P.; Gualtieri, G.J.; Kammlott, G.W.; Malm, D.L. On the mechanism of silver and copper sulfidation by atmospheric H_2S and OCS. *Corros. Sci.* **1985**, *25*, 1163–1180. [[CrossRef](#)]
16. Kong, D.; Dong, C.; Xu, A.; Man, C.; He, C.; Li, X. Effect of sulphide concentration on copper corrosion in anoxic chloride-containing solutions. *J. Mater. Eng. Perform.* **2017**, *26*, 1741–1750. [[CrossRef](#)]
17. Su, W.; Lv, W.; Liu, Z.; Zhang, Z. Corrosion of copper exposed to Zhanjiang and Zhuhai atmospheric environments. *Anti-Corros. Methods Mater.* **2017**, *64*, 286–292. [[CrossRef](#)]
18. Fujimoto, S.; Umemura, H.; Shibata, T. Atmospheric corrosion of electroplated cu thin film in moist oxygen environment. *ECS Trans.* **2006**, *1*, 243–247. [[CrossRef](#)]

19. Araban, V.; Kahram, M.; Rezakhani, D. Evaluation of copper atmospheric corrosion in different environments of Iran. *Corros. Eng. Sci. Technol.* **2016**, *51*, 498–506. [CrossRef]
20. FitzGerald, K.P.; Nairn, J.; Skennerton, G.; Atrons, A. Atmospheric corrosion of copper and the colour, structure and composition of natural patinas on copper. *Corros. Sci.* **2006**, *48*, 2480–2509. [CrossRef]
21. Kong, D.C.; Dong, C.F.; Fang, Y.H.; Xiao, K.; Guo, C.Y.; He, G.; Li, X.G. Copper corrosion in hot and dry atmosphere environment in Turpan, China. *Trans. Nonferrous Met. Soc. China* **2016**, *26*, 1721–1728. [CrossRef]
22. Lopesino, P.; Alcántara, J.; Fuente, D.; Chico, B.; Jiménez, J.; Morcillo, M. Corrosion of copper in unpolluted chloride-rich atmospheres. *Metals* **2018**, *8*, 866. [CrossRef]
23. Yan, F.; Li, X.; Jiang, B.; Lin, D.; Fu, M.; Li, W. Initial corrosion behaviour of pure copper in atmospheric environment. *IOP Conf. Ser. Earth Environ. Sci.* **2019**, *384*, 012039. [CrossRef]
24. Zhang, F.; Örnek, C.; Liu, M.; Müller, T.; Lienert, U.; Ratia-Hanby, V.; Carpen, L.; Isotahdon, E.; Pan, J. Corrosion-induced microstructure degradation of copper in sulphide-containing simulated anoxic groundwater studied by synchrotron high-energy X-ray diffraction and ab-initio density functional theory calculation. *Corros. Sci.* **2021**, *184*, 109390. [CrossRef]
25. Saha, D.; Pandya, A.; Singh, J.K.; Paswan, S.; Singh, D.D.N. Role of environmental particulate matters on corrosion of copper. *Atmos. Pollut. Res.* **2016**, *7*, 1037–1042. [CrossRef]
26. Hedin, A.; Johansson, A.J.; Lilja, C.; Boman, M.; Berastegui, P.; Berger, R.; Ottosson, M. Corrosion of copper in pure O₂-free water. *Corros. Sci.* **2018**, *137*, 1–12. [CrossRef]
27. Sharma, S.P. Reaction of copper and copper oxide with H₂S. *J. Electrochem. Soc.* **1980**, *127*, 21–26. [CrossRef]
28. Wu, T.; Zhou, Z.; Xu, S.; Xie, Y.; Huang, L.; Yin, F. A corrosion failure analysis of copper wires used in outdoor terminal boxes in substation. *Eng. Failure Anal.* **2019**, *98*, 83–94. [CrossRef]
29. Thethwayo, B.M.; Garbers-Craig, A.M. Laboratory scale investigation into the corrosion of copper in a sulphur-containing environment. *Corros. Sci.* **2011**, *53*, 3068–3074. [CrossRef]
30. Chen, J.; Qin, Z.; Martino, T.; Shoesmith, D.W. Non-uniform film growth and micro/macro-galvanic corrosion of copper in aqueous sulphide solutions containing chloride. *Corros. Sci.* **2017**, *114*, 72–78. [CrossRef]
31. Lu, X.; Liu, Y.; Liu, M.; Wang, Z. Corrosion behaviour of copper T2 and brass H62 in simulated Nansha marine atmosphere. *J. Mater. Sci. Technol.* **2019**, *35*, 1831–1839. [CrossRef]
32. Schindelholz, E.J.; Cong, H.; Jove-Colon, C.F.; Li, S.; Ohlhausen, J.A.; Moffat, H.K. Electrochemical aspects of copper atmospheric corrosion in the presence of sodium chloride. *Electrochim. Acta.* **2018**, *276*, 194–206. [CrossRef]
33. Deutscher, R.L.; Woods, R. Characterization of oxide layers on copper by linear potential sweep voltammetry. *J. Appl. Electrochem.* **1986**, *16*, 413–421. [CrossRef]
34. Tran, T.T.M.; Fiaud, C.; Sutter, E.M.M.; Villanova, A. The atmospheric corrosion of copper by hydrogen sulphide in underground conditions. *Corros. Sci.* **2003**, *45*, 2787–2802. [CrossRef]
35. Tran, T.T.M.; Fiaud, C.; Sutter, E.M.M. Oxide and sulphide layers on copper exposed to H₂S containing moist air. *Corros. Sci.* **2005**, *47*, 1724–1737. [CrossRef]
36. Nielsen, B.C.; Doğan, Ö.N.; Howard, B.H. Effect of temperature on the corrosion of Cu-Pd hydrogen separation membrane alloys in simulated syngas containing H₂S. *Corros. Sci.* **2015**, *96*, 74–86. [CrossRef]
37. Cai, L.; Chen, M.; Wang, Y.; Chen, C.; Zhang, L.; Zhou, H.; Wu, L.; Yan, Y. Electrochemical corrosion behaviour of bronze materials in an acid-containing simulated atmospheric environment. *Mater. Corros.* **2019**, *71*, 464–473. [CrossRef]
38. Yu, X.; Wang, Z.; Lu, Z. In situ investigation of atmospheric corrosion behaviour of copper under thin electrolyte layer and static magnetic field. *Microelectron. Reliab.* **2020**, *108*, 113630. [CrossRef]
39. Bellakhal, N.; Draou, K.; Brisset, J.L. Electrochemical investigation of copper oxide films formed by oxygen plasma treatment. *J. Appl. Electrochem.* **1997**, *27*, 414–421. [CrossRef]
40. *ASTM Standard D-130-80, Part 23*; American Society for Testing and Materials: West Conshohocken, PA, USA, 1981; p. 104.
41. Wang, H.; Xie, J.; Yan, K.P.; Duan, M.; Zuo, Y. The nucleation and growth of metastable pitting on pure iron. *Corros. Sci.* **2009**, *51*, 181–185. [CrossRef]
42. Persson, D.; Leygraf, C. In situ infrared reflection absorption spectroscopy for studies of atmospheric corrosion. *J. Electrochem. Soc.* **1993**, *140*, 1256–1260. [CrossRef]
43. Zhao, W.; Babu, R.P.; Chang, T.; Odnevall, I.; Hedström, P.; Johnson, C.M.; Leygraf, C. Initial atmospheric corrosion studies of copper from macroscale to nanoscale in a simulated indoor atmospheric environment. *Corros. Sci.* **2022**, *195*, 109995. [CrossRef]
44. Paul, A.M.; Sajeev, A.; Nivetha, R.; Gothandapani, K.; Bhardwaj, P.; Raghavan, V.; Jacob, G.; Sellapan, R.; Jeong, S.K.; Grace, A.N. Cuprous oxide/graphitic carbon nitride (g-C₃N₄) nanocomposites for electrocatalytic hydrogen evolution reaction. *Diamond Relat. Mater.* **2020**, *107*, 107899. [CrossRef]
45. Shanghai Institute of Organic Chemistry of CAS. Chemistry Database. 1978–2022. Available online: <http://www.organchem.csdb.cn>. (accessed on 1 February 2022).
46. Li, K.; Chen, Z.; Li, J.; Sun, X.; Xu, F.; Xu, L. Corrosion mechanism of copper immersed in ammonium sulphate solution. *Mater. Corros.* **2018**, *69*, 1597–1608. [CrossRef]
47. Chialvo, M.R.G.; Marchiano, S.L.; Arvía, A.J. The mechanism of oxidation of copper in alkaline solutions. *J. Appl. Electrochem.* **1984**, *14*, 165–175. [CrossRef]